Geotechnical Aspects of Underground Construction in Soft Ground – Viggiani (ed)
© 2012 Taylor & Francis Group, London, ISBN 978-0-415-68367-8

Analysis of convergence data and 3D numerical modelling of tunnels excavated in fine-grained soils

P. Perazzelli & T. Rotonda
Department of Structural and Geotechnical Engineering, Sapienza University, Rome, Italy

D. Boldini
Department of Civil, Environmental and Material Engineering, University of Bologna, Bologna, Italy

A.M. Ajmone-Cat
Astaldi S.p.A., Rome, Italy

P.M. Gianvecchio
CO.MERI S.p.A., Rome, Italy

ABSTRACT: This paper focuses on the convergence measurements of twin motorway tunnels under excavation in a Pliocene formation in the South of Italy. The tunnels are driven full face, with a cross-section of 120 m^2, by means of a conventional excavation method, up to a maximum depth of 120 m. The primary lining is an open arch made up of shotcrete and steel sets; the definitive lining consists of concrete cast in three different stages. Convergence measurements were analyzed on the basis of the curve-fitting technique proposed by Sulem et al. (1987). Then, the influence on tunnel deformation of overburden and lining construction sequence is investigated. Finally, the role of the primary and final linings in reducing tunnel convergence is investigated by means of a three-dimensional stress-strain analysis, performed with FLAC3D code.

1 INTRODUCTION

Modern tunnelling methods include ground displacement monitoring as an essential part of the construction: it allows confirmation of design assumptions and provides a basis for changes in the excavation sequence and support methods. The paper presents convergence measurements carried out at two parallel motorway tunnels under excavation in a fine-grained formation in the South of Italy.

Convergence measurements were analyzed accordingly to the model proposed by Sulem et al. (1987), which relates tunnel displacements to both face distance and time-dependent behaviour of the soil. The influence of the lining construction sequence, as well as that of tunnel overburden, are discussed. Three-dimensional numerical stress analyses, using the FLAC3D code, are also presented, in order to investigate the role of different primary support systems and the construction sequence of final lining on the tunnel deformation.

2 SANTA MARIA TUNNELS

The Santa Maria twin tunnels are part of the new motorway route 'SS 106 Jonica', under construction on behalf of ANAS S.p.A.. The motorway crosses the South of Italy running along the Jonic Sea, between the towns of Taranto and Reggio Calabria. The tunnels take the name from the Santa Maria hill, in the Catanzaro countryside, through which they are excavated.

The tunnels, which are currently under construction, are 1.3 km long. They are identified as "North tunnel", which runs towards Taranto, and "South tunnel", which runs towards Reggio Calabria.

The twin tunnels are excavated in a Pliocene formation, mostly consisting of silty clay. They are driven full face using a conventional excavation method, up to a maximum depth of 120 m. The tunnel diameter is about 13.0 m, which corresponds to a cross-section of 120 m^2, and the minimum clearance between the tunnels is 20 m.

An open primary lining made up of shotcrete and steel sets has been adopted. The concrete final lining has been cast in three different stages, i.e. the sidewall, invert and vault of the tunnel section.

Careful monitoring is being carried out in order to ensure compliance with construction quality requirements, verify design assumptions and adapt primary lining. Regular measurement of tunnel displacements is carried out. In a few sections along the tunnel extension also the load in the lining is monitored.

2.1 *Geological and geotechnical outlines*

The Santa Maria hill is formed by two Pliocene formations (Fig. 1). In the upper part of the hill there is a formation denominated 'Asa', composed of alternating layers of sandstones (decameter thickness) and loose sand (centimetric thickness). At the bottom of the hill there is a lithological unit denominated 'Ags', composed of alternating levels of gray blue silty clay (multidecameter), crossed locally by layers of sand and silt, and of decameter levels of silty-sandy clay.

The tunnels are mainly excavated through the Ags formation. During the design stage, geotechnical investigations were carried out only in areas near the tunnel entrance and in areas subject to higher overburdens. During the excavation, samples have been also collected from the tunnel face, in order to improve the knowledge of soil properties at the tunnel depth.

Along the entire route, the tunnels pass through a fine-grained soil with a high percentage of silt (on average up to 50%) and a variable percentage of clay and sand. In some limited areas the percentage of the sand increases up to 40% (Fig. 2).

A summary of the physical and mechanical properties of the soil sampled at the tunnel face is shown in Table 1. No significant variations are recorded between the two tunnels. Plastic and liquid limits vary in the intervals, respectively, 20–25% and 30–50% (Fig. 3). Values of water content, in the interval between 20 and 30%, are close to the plastic limit. Using Casagrande's classification, the fine fraction of the soil sampled can be classified as an inorganic clay of medium plasticity.

Compressibility was investigated in the laboratory by means of oedometer compression tests: compressibility and swelling indexes exhibit values in the intervals, respectively, 0.06–0.12 and 0.020–0.055.

Triaxial, as well as direct shear tests, were also carried out. Very high scattered values of strength parameters were obtained along the tunnels: the peak cohesion varies in the interval 20–50 kPa, while the peak friction angle varies in the interval 25°–35°. The larger values of friction angle, associated to the lower values of cohesion, were obtained for samples with a higher percentage of sand.

Limited data is available on the water table level and on pore pressure distribution in the excavated

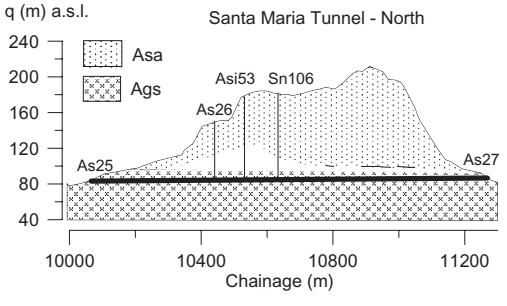

Figure 1. Schematic geological profile of the Santa Maria tunnel (North) (the thick line represents the tunnel). Vertical boreholes are also shown.

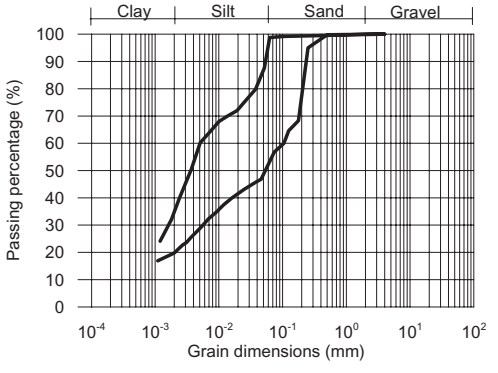

Figure 2. Two limit grain-size distributions of soil samples collected at the tunnel face.

Table 1. Properties of the soil.

Properties	Min-Max
Total unit weigth γ(kN/m^3)	20.8–21.4
Dry unit weigth γ_d (kN/m^3)	17.2–19.3
Solid unit weigth γ_s (kN/m^3)	26.4–26.5
Void index e	0.39–0.56
Natural water content w (%)	21–32
Liquid limit w_l (%)	30–50
Plastic limit w_p (%)	18–25
Saturation degree S_r (%)	91–99
Clay fraction CF (%)	13–41
Compression index C_c	0.06–0.12
Swelling index C_s	0.02–0.055
Peak cohesion c'_p (kPa)	18–51
Peak friction angle φ'_p (°)	25–35

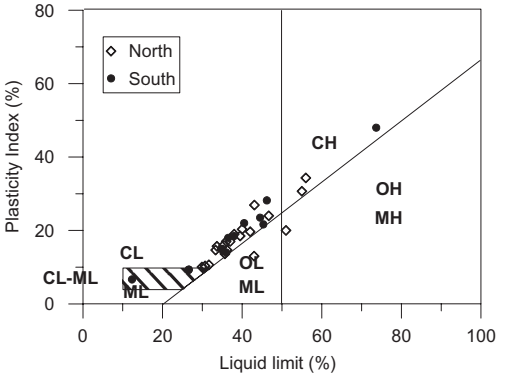

Figure 3. Casagrande's classification of the soil.

formations. In the design stage water table was assumed to be close to the bottom of Asa formation, i.e. at about 20 m above the tunnel crown. The hydraulic conductivity estimated from oedometer compression tests was shown to be very low, varying in the interval 10^{-11}–10^{-10} m/s.

The high percentage of silt and the high disturbance of samples taken at the tunnel face, did not allow in oedometer compression tests a reasonable estimation of the preconsolidation pressure, therefore the overconsolidation ratio is not directly known.

3 DESIGN AND CONSTRUCTION

The design of the tunnels was based on the observational ADECO-RS approach (Lunardi 2000). Different typology of primary linings were applied to specific geotechnical conditions; the effectiveness of the adopted solution are checked by comparing the monitored convergences to predetermined reference values.

Figure 4 shows the typical cross-section of the tunnel with the primary lining consisting of an open ring of shotcrete (thickness of 0.20–0.30 m) and steel sets (2 coupled bars among the types IPN 160–180–220). The unsupported span has a length of up to 1.0–1.2 m for the more ordinary excavation sections (section area of 120 m^2), while it decreases up to 0.75 m in the case of larger excavation sections (section area of 180 m^2), planned as security stop areas.

Face reinforcement consists of 18 m long fiberglass bolts, installed every 10–12 m of face advancement, thus resulting in a overlap of 6 m. In some cases face bolting, with a maximum density of 1 bolts/m^2, is adopted.

The concrete final support (thickness of 0.8–1.0 m) is cast in three separate stages, the cast

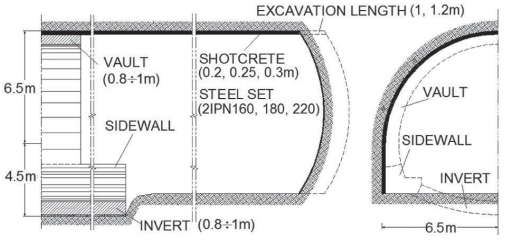

Figure 4. Typical cross—and longitudinal section of the tunnel.

length being typically 6–12 m. Firstly, concrete at the sidewall (Fig. 4) is constructed at a maximum distance from the face of 24–30 m; then, the invert is cast typically 6–12 m behind the sidewall; finally, the arch lining is closed by the vault, generally 60–70 m from the face.

The advance rate of the tunnel is between 1.5 and 3.0 m/day.

4 ANALYSIS OF CONVERGENCE MEASUREMENTS

The construction process is monitored mainly through the geodetic survey of displacements at the tunnel wall. Monitoring sections include 5 targets installed according to a typical scheme: three at the top-heading and two at each sidewall.

A monitoring section is installed every excavation cycle, i.e. 12 ÷ 18 m; they should be placed no more than 1 m from the face. Monitoring is interrupted when the permanent concrete lining is cast.

For shorter distances from the face, i.e. less than 15 m (almost 1 tunnel diameter), one measurement per day is carried out, while for longer distances, the frequency decreases to 2 or less measurements per week.

4.1 *Data convergence interpretation*

The interpretation of convergence data was based on the regression model proposed by Sulem et al. (1987). The model supposes that the tunnel closure C is influenced both by the face distance and time dependent behaviour of the soil:

$$C(x,t) = C_{\infty}\left\{1-\left[\frac{X}{x+X}\right]^2\right\}\left\{1+m\left[1-\left(\frac{T}{t+T}\right)^n\right]\right\} \quad (1)$$

where x is the distance of the monitoring section from the face and t is the time elapsed since the face crossed the control section. The parameter C_{∞} represents the closure corresponding to an infinite advancement rate; the parameter X corresponds to

the face effect (it is related to the plastic radius R); parameters m, T and n describes the time effect; the quantity $C(1 + m)$ represents the closure at infinite distance and time.

The measured convergence is a fraction of the actual total closure; it generally depends on the face distance x_0 at the "zero" reading and on the time t_0 elapsed since the face crossed the monitoring section until the "zero" reading:

$$\Delta C(x_i,t_i) = C(x_i,t_i) - C(x_0,t_0) \qquad i = 1,k \qquad (2)$$

Solving the non linear equation (1) on the basis of the collected data $\Delta C_i(x_i,t_i)$, for example by means of a minimum squares regression technique, allows the estimation of the regression parameters.

As suggested by various authors (Sulem et al. 1987, Boldini et al. 2002), the parameter n was fixed at the value of 0.3 in order to reduce the ill-conditioning of the set of k equations (2).

In the regressions analysis convergence data collected during sidewall and invert installations were not considered. In this way the influence of invert excavation and variation of stiffness support on the regression results are minimized.

In Figure 5 three examples of convergence fitting of the L_1 control length are represented. The regression model is shown to be able to fit the measurements corresponding to different excavation sequences. Moreover the increase in convergence during breaks in excavation is also accurately matched by the model.

Parameters determined by the regression analysis of convergence measurements from the control length L_1 are reported in Figure 6 as a function of the tunnel chainage. The magnitude of the parameter C_∞ is often lower than 0.150 m, corresponding to an average deformation nearly 1% (L_1 = 14 m); it increases as the tunnel proceeds, probably due to the related overburden increment. The length X varies between 5 and 15 m, and it is frequently close to 6.5 m, i.e. equal to the tunnel radius. The characteristic time T is widely scattered in the range 1–35 days. The non-dimensional parameter m also shows a large range of variation, between 0 and 4.

From these results it seems inadequate to define a single behaviour model in term of convergence, representative of all conditions encountered. On the other hand the regression model makes it possible to estimate the tunnel closure before the "zero" reading $C(x_0, t_0)$, allowing the comparison of measurements collected in different monitoring stations.

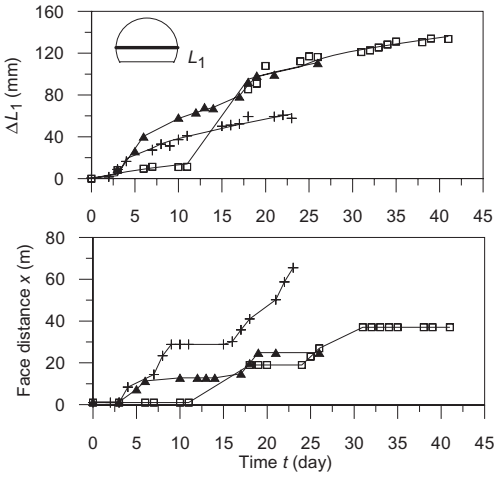

Figure 5. Examples of curve fitting (continuous line) of convergence measurements ΔL_1 (symbols) with time (on the top) at three monitoring sections. At the bottom the distance of the monitoring section from tunnel face versus time is shown.

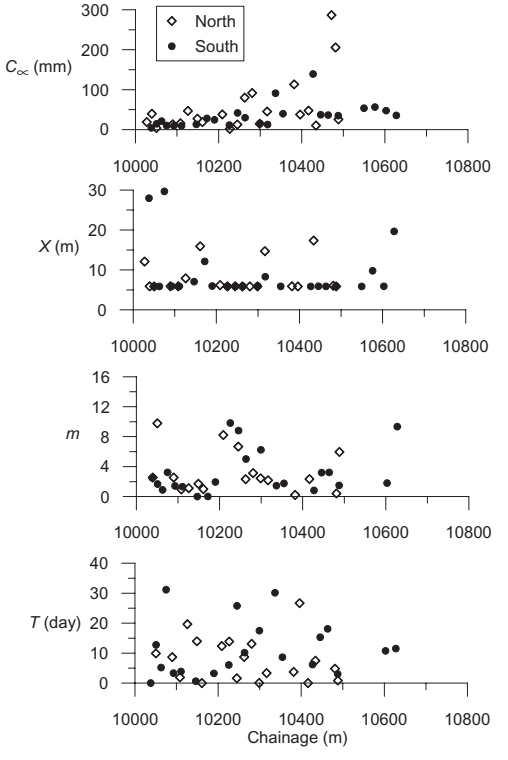

Figure 6. Regression parameters from eq. (1) obtained from the convergence data of the horizontal control length L_1 for both North and South tunnels.

4.2 *The influence of the sequential installation of definitive lining*

The construction sequence of the various structural elements of the final lining is relevant in the development of the convergence.

Figures 7a and 7b illustrate, as an example for three monitoring sections, the measured closure of the horizontal control length L_1 with time in relation to the history of the distance of the monitoring section from the face. The distance of the sidewall and the invert installation from the section itself is also shown (Figs. 7c, and 7d, respectively). The installation of the final support elements at the sidewall (i.e. distance equal to zero in Fig. 7c) causes the closure of L_1 to end, even if the arch of the primary support is not closed at the foot.

The measurements of the oblique tunnel convergences also show the same behaviour as the horizontal convergence. However, the vertical displacement at the crown continues to increase overtime until reaching an asymptotic value.

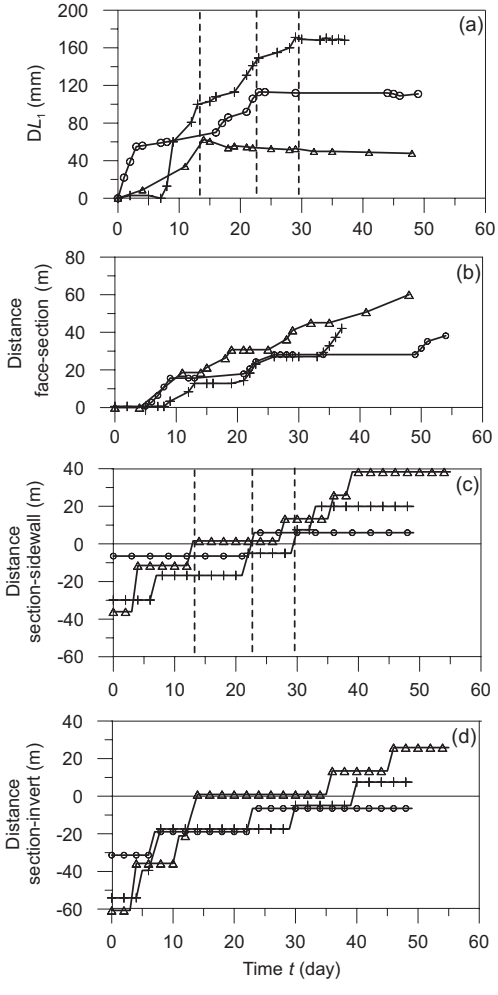

Figure 7. Time histories of: a) the measured convergence of the horizontal closure L_1; b), c) and d) the progression of the face, sidewall and invert concrete, respectively, with reference to the control section position. The vertical lines refers to the time of casting of the sidewall.

4.3 *Comparison of data at different monitoring sections*

Generally, there are many factors that affect tunnel convergence: geometry and depth of tunnel; geotechnical properties and hydraulic conditions; the characteristics of primary and definitive supports; excavation sequence, especially in the case of twin tunnels.

Comparison of monitored data was carried out without taking into account the variability of the mechanical properties and hydraulic condition of the soil encountered by the tunnel. Differences in the primary support and in the sequence of installation of final lining were also assumed as negligible.

The comparison focused on the influence of the tunnel depth and distinguished the data from the two tunnels, with the aim of assessing eventual interaction effects.

In order to evaluate a dissymmetry of the tunnel deformation, the convergence from two oblique control lengths, ΔL_2 and ΔL_3 (Fig. 8), was considered. In Figure 8 such measurements, normalized

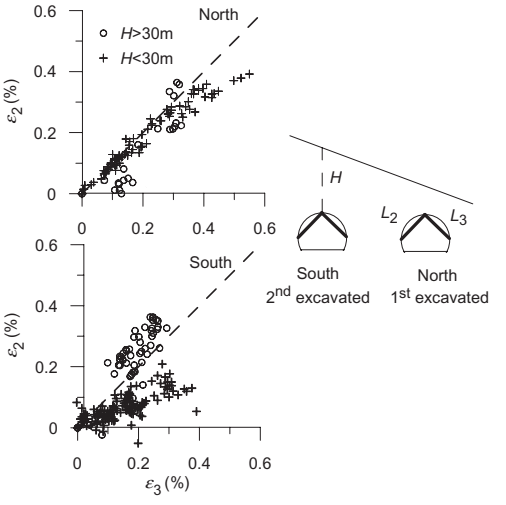

Figure 8. Comparison between the deformations of oblique control lengths for both tunnels. A different symbol is used to distinguish between data recorded at tunnel sections below and above 30 m of overburden.

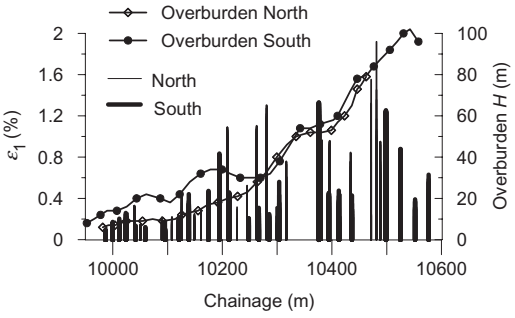

Figure 9. Deformation of the horizontal control length (bars) and overburden (symbols) along both the tunnel axes.

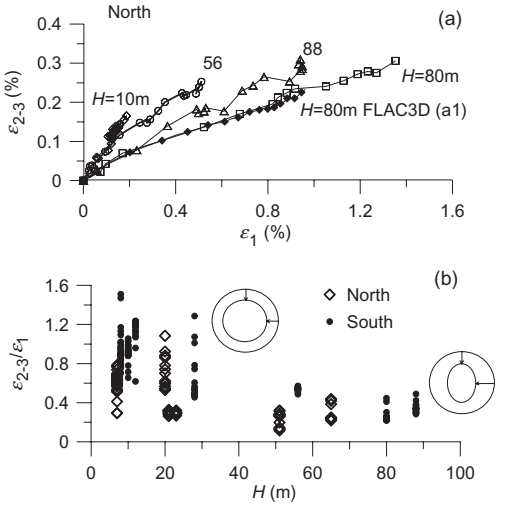

Figure 10. (a) Mean deformation $\varepsilon_{2\text{-}3}$ of the two oblique control lengths against the horizontal deformation ε_1 from several monitoring sections (open symbols) and from FLAC3D analyses (full symbols) at different overburden H. (b) Ratio between measured deformations of oblique and horizontal control lengths related to overburden H.

to the initial basis length ($L_2 = L_3 = 9$ m) and indicated as ε_2 and ε_3, are plotted for several monitoring sections. If tunnel cover H is high (>30 m), an almost symmetric shape of tunnel closure is displayed in both tunnels, even though data are largely scattered. On the other hand, at lower tunnel cover ($H < 30$ m) the convergence of the control length ΔL_3 is always larger than ΔL_2.

The dissymmetry in the tunnel closure could be ascribed to the rotation of the original principal stresses due to the slope or to the sequence of tunnel excavation. As the dissymmetry in the closure at the lower cover ($H < 30$ m) is negligible in the North tunnel (firstly excavated) and more marked in the South tunnel (later excavated), it suggests a higher influence of the sequence of tunnel excavation.

In Figure 9 the deformation of the horizontal closure, indicated as ε_1, as well as the overburden H, are represented as a function of the tunnel chainage. Deformation values from the North and South tunnels are quite similar. The horizontal closure, even though very scattered, reasonably increases with the overburden. The average increment of ε_1 with overburden is 0.018%/m, corresponding to a horizontal closure increase of 0.0025 m per 1 m of overburden.

It should be noted that in the larger excavation section (180 m^2), the deformation of the horizontal convergence is very similar to that of the ordinary section.

Comparison between ε_1 and the average value of ε_2 and ε_3, for several monitoring sections of the North tunnel is shown in Figure 10a. Convergence increases during the excavation, maintaining a constant ratio, which differs with depth. Figure 10b shows the correlation between depth and ratio of oblique to horizontal closure deformations, which can be considered as a measure of the oval shape. At lower overburden this ratio differs significantly, with an average closer to 1.0, while at larger overburden ($H > 40$ m) it decreases significantly. The tunnel deformation at lower depth maintains a homothetic shape, while at larger depth an oval-shaped closure, with the maximum closure in the horizontal direction, occurs. This evidence could be related to the incomplete closure of the primary support.

5 STRESS-STRAIN NUMERICAL ANALYSIS

Convergence measurements showed that the installation distance of the primary lining strongly affect the tunnel behaviour. Moreover, placement of the lining at the sidewall (also without invert) seems to have a key role in reducing tunnel displacement (Fig. 7).

In order to better understand these phenomena, comparative stress analyses, simulating the sequence of lining installation, were carried out. Analyses were performed with the commercial finite difference code FLAC3D (Itasca 2006) in the three dimensional domain.

5.1 *Numerical models*

The analyses were performed maintaining constant the tunnel overburden (H = 80 m) and soil properties.

The soil was modeled as an elastic perfectly plastic material, obeying the Mohr-Coulomb yielding criterion. Cohesion and friction angle were assumed equal to $c' = 30$ kPa and $\varphi' = 30°$, respectively. A non associated plasticity flow rule, characterized by the null value for the dilation angle ψ' was considered. As soil stiffness was not directly investigated, reasonable values for the elastic constant were assumed, i.e. $E' = 400$ MPa and $\nu' = 0.3$. The coefficient of earth pressure at rest K_0 was chosen equal to 1, a typical value for deep tunnels.

The analyses were performed in undrained conditions in the effective stress domain. According to the design assumptions, water table was fixed at 20 m above the tunnel crown.

The soil and water properties used in the analyses are summarized in Table 2.

Due to the symmetry in the vertical plane of the tunnel axis, only one half of the entire domain was modeled. The calculation mesh, consisting of 271680 nodes and 260967 zones, is reported in Figure 11. The component of displacement perpendicular to the vertical boundary planes was restrained. All components of the displacement were restrained at the bottom of the model.

The excavation process was simulated by applying the following procedure: for each excavation step, equal to 1 m, a set of soil elements are changed into null elements; the excavated soil slice remains unsupported while the primary lining is installed 1 m behind. The primary lining consists of shotcrete, modeled as elastic shells, and steel sets, modeled as elastic beam elements. The lining elements were considered perfectly adhered to the soil.

In order to take into account the maturation process of shotcrete, its Young modulus E_s was increased during face advancement, while a constant value of the Poisson ratio of 0.25 was assumed. An empirical relationship (Chang 1994, Graziani et al. 2005) was assumed to describe the dependence of E_s on time:

$$\frac{E_s(t)}{E_{s,28}} = c_1 \exp\left\{\left(\frac{c_2}{t^{c_3}}\right)\right\} \tag{3}$$

where c_1, c_2 and c_3 are equal, respectively, to 1.062, –0.446, 0.6 and the Young modulus at 28 days of maturation was fixed at 20 GPa.

The beam elements consisted of two coupled IPN standard steel beams (Tab. 3).

Three different types of primary linings were considered, i.e. minimum, average and maximum stiffness, as proposed in the design (Tab. 3).

The permanent lining elements considered in the analysis were sidewall and invert concrete, while the vault element was not included. The structural elements were modeled through elastic brick elements, characterized by Young modulus and Poisson ratio equal to 25 GPa and 0.25, respectively. A perfect adherence of the structural elements to the soil was assumed.

Sidewall and invert elements were installed every 6 m, as in the actual construction. Two different installation distances from the face were considered: 12 and 24 m (corresponding to minimum distances from the face of 6 and 18 m after the casting, respectively). Two hypotheses of installations were investigated: installation of concrete at the sidewall only (cases a2, a3 in Tab. 3) and installation of both sidewall and invert (cases a4, a5 in

Table 2. Relevant parameters adopted in the numerical analyses.

Soil	
Dry unit weigth γ_d (kN/m^3)	18
Porosity n	0.35
Young modulus E' (Mpa)	400
Poisson ratio v	0.3
Friction angle φ' (°)	30
Cohesion c' (kPa)	30
Dilation angle Ψ' (°)	0
Water	
Unit weigth γ_w (KN/m^3)	10
Bulk modulus K_w (Gpa)	2
Maximum suction s (kPa)	200
Initial State	
Height of water table on the tunnel crown h_w (m)	20
Coefficient of earth pressure at rest K_0	1

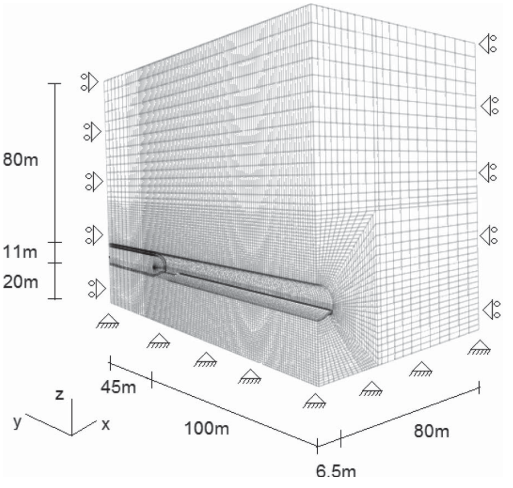

Figure 11. Calculation mesh including boundary constraints.

Table 3. Lining characteristics adopted for the various analyses.

Primary lining	(min)*	(average)	(max)*
Shotcrete thick. (m)	0.2	0.25	0.3
Steel sets	2IPN160	2IPN180	2IPN180
Definitive lining			
Installation length (m)		6	
Maximum installation distance (m) for:			
	(a1)	(a2)	(a3)	(a4)	(a5)
Sidewall	∞	12	24	12	24
Invert	∞	∞	∞	12	24
Vault	∞	∞	∞	∞	∞

*primary linings investigated only in the condition (a3)

Tab. 3). The case of definitive lining installed at infinite distance was also investigated (case a1 in Tab. 3).

5.2 *Results*

The L_1 horizontal convergence and the vertical displacement at the crown from the analyses are reported in Figure 12. The installation of sidewall and invert concrete at long distances from the face (a1) and at the maximum distance of 24 m (a5) gives a horizontal deformation ε_1 between 0.7% (a5) and 1% (a1), comparable with the monitoring data at similar overburden (Fig. 9).

Also the deformation ε_{2-3} from numerical analyses shows a good agreement with the measured values (Fig. 10a). Furthermore the analyses provide a ratio $\varepsilon_{2-3}/\varepsilon_1$ varying from 0.28 (a5) to 0.25 (a1), consistent with the non homothetic tunnel deformation measured at higher overburdens (Fig. 10b).

The behaviour of tunnel deformation when only sidewall concrete is installed (a1, a2 and a3) is also qualitatively confirmed by the numerical investigations. Figure 12a shows that, at the installation distance of 24 m (a3), horizontal convergence stops increasing when the sidewall concrete reaches the reference section, at 18 m (i.e. minimum installation distance for this case). Figure 12b, on the contrary, shows that the vertical displacement at the crown is still increasing at the same distance, attaining a final value only at a larger face distance (24 m). The noticeable effect of sidewall casting is confirmed by comparing the maximum values of displacements obtained at different installation distances (a1, a2 and a3). Even though the sidewall is installed at 24 m (almost 2 times tunnel diameter) from the face (case a3), convergence strongly reduces with respect to the infinite installation distance (case a1) (Fig. 12).

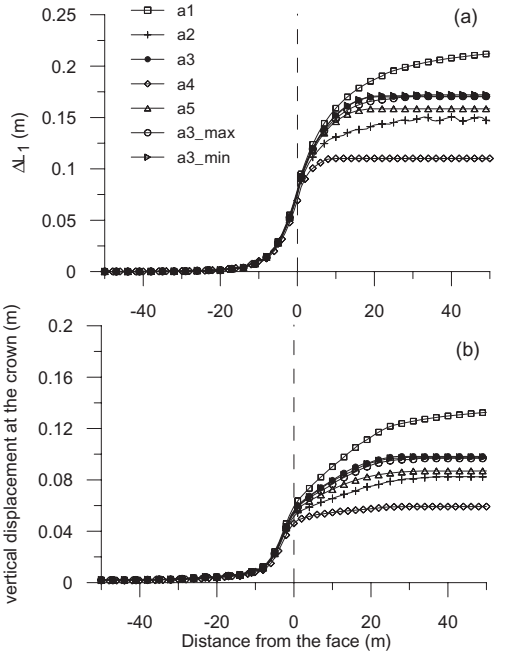

Figure 12. (a) Shortening of the horizontal control length L_1 and (b) vertical displacement at the crown resulting from the numerical stress analyses.

Figure 12 also shows that, for both the horizontal convergence and the vertical displacement at the crown, there are no significant differences if sidewall is cast alone (a3) or together with the invert (a5), when the installation distance is longer than 24 m. At shorter installation distance (12 m), the placement of the sidewall alone (a2) and with the invert (a4) produces different results: the invert installation shows a sharp reduction in the increase of convergence as the face advances.

The role of invert installation can reasonably be assumed: closure of primary lining with the invert strongly increases the overall lining stiffness. On the contrary, the important increase in stiffness following the sidewall installation is less apparent.

The influence of the installation of primary linings with different stiffnesses (minimum, average and maximum), in the hypothesis that only the sidewall is cast at the distance of 24 m (a3), is also shown in Figure 12. In these analyses, at least for the investigated soil properties and tunnel depth, results show that in order to reduce tunnel convergences it is not possible to separate the effects of an increase in the primary lining stiffness, from those of a reduction in the distance between the primary and definitive linings.

6 CONCLUSIONS

In this paper monitoring data from two tunnels excavated in a fine-grained formation are analysed and compared with the results of 3D numerical simulations.

The regression model of Sulem et al. (1987) proved to be a reliable instrument in the comparison of convergence data measured at different face distances and relative to different excavation sequences.

The detailed analysis of the convergence measurements of the two tunnels suggested some evidence from the interaction between lining and soil. Analyses showed that tunnel overburden, as well as the different components of the definitive lining (at sidewall and invert), clearly affect the intensity of tunnel deformation. At the higher depth the tunnel shape does not depend on the overburden: the higher horizontal closure is presumed to be influenced by the low stiffness of the primary lining, working as an open arch. The concrete at the sidewall increases the stiffness at the foot of the primary lining, so reducing the effects of punching.

Horizontal and vertical displacements from 3D numerical analyses were in accordance with the monitoring data.

The numerical stress analyses highlighted (in accordance with the monitoring data) the relevant role of the installation distance of the different structural elements of the linings.

Results from convergence measurements suggest that the effects of the excavation sequence between the two tunnels requires further analyses.

ACKNOWLEDGEMENT

The contribution of ANAS S.p.A. (the developer of the motorway route) and Astaldi S.p.A. (the main contractor) to the promotion of scientific knowledge is greatly appreciated. Thanks to Astaldi S.p.A. are also due for allowing site access and their financial contribution to this research.

REFERENCES

Boldini, D., Graziani, A. & Ribacchi, R. 2005. Raticosa tunnel, Italy: characterization of tectonized clay-shale and analysis of monitoring data and face stability. *Soils and Foundations* 44(1): 59–71.

Chang, Y. 1994. Tunnel support with shotcrete in weak rock—A rock mechanics study. Ph.D. Thesis, Division of Soil and Rock Mechanics, Royal Institute of Technology, Stockholm, Sweden.

Graziani, A., Boldini, D. & Ribacchi, R. 2005. Practical estimate of deformations, loads and stress relief factors for deep tunnels supported by shotcrete. *Rock Mech. Rock Engng.* 35(5): 345–372.

Itasca 2006. *Flac3D, Vers. 3.1*. Minneapolis

Lunardi, P. 2000. The design and construction of tunnels using the approach based on the analysis of controlled deformation in rocks and soils. *Tunnels & Tunnelling International* 5: 3–29.

Sulem, J., Panet, M. & Guenot, A. 1987. Closure analysis in deep tunnels. *Int. J. Rock Mech. Min. Sci. & Geomech. Abstr.* 24(3): 145–154.